Published in final edited form as:
Cell Rep. 2015 January 6; 10(1): 29–38. doi:10.1016/j.celrep.2014.12.001.

An autoregulatory mechanism imposes allosteric control on the V(D)J recombinase by histone H3 methylation

Chao Lu[1,2], **Alyssa Ward**[1], **John Bettridge**[1], **Yun Liu**[1,3], and **Stephen Desiderio**[1,*]

[1]Department of Molecular Biology and Genetics and Institute for Cell Engineering, The Johns Hopkins University School of Medicine, Baltimore, MD 21205

[2]Department of Physiology and Pathophysiology, School of Basic Medical Sciences, Fudan University, Shanghai 200032, China

SUMMARY

V(D)J recombination is initiated by a specialized transposase consisting of the subunits RAG-1 and RAG-2. The susceptibility of gene segments to DNA cleavage by the V(D)J recombinase is correlated with epigenetic modifications characteristic of active chromatin, including trimethylation of histone H3 on lysine 4 (H3K4me3). Engagement of H3K4me3 by a plant homeodomain (PHD) in RAG-2 promotes recombination in vivo and stimulates DNA cleavage by RAG in vitro. We now show that H3K4me3 acts allosterically at the PHD finger to relieve autoinhibition imposed by a separate domain within RAG-2. Disruption of this autoinhibitory domain was associated with constitutive increases in recombination frequency, DNA cleavage activity, substrate binding affinity and catalytic rate, thus mimicking the stimulatory effects of H3K4me3. Our observations support a model in which allosteric control of RAG is enforced by an autoinhibitory domain whose action is relieved by engagement of active chromatin.

INTRODUCTION

During lymphocyte development the genes encoding antigen receptors are assembled from discrete gene segments by V(D)J recombination. This process is initiated by the proteins RAG-1 and RAG-2, which together cleave DNA at recombination signal sequences (RSSs) that flank the participating gene segments (Gellert, 2002; Schatz and Swanson, 2011). There are two classes of RSS, termed 12-RSS and 23-RSS, in which heptamer and nonamer elements are separated by spacers of 12 bp or 23 bp, respectively. DNA cleavage by RAG

[*]Corresponding author: telephone (410) 955-4735, sdesider@jhmi.edu.
[3]Current address: Center for Epigenetics, Institute for Basic Biomedical Sciences, The Johns Hopkins University School of Medicine, Baltimore, MD 21205

AUTHOR CONTRIBUTIONS

C.L., A.W. and J.B. conceived of, designed and performed experiments. C.L., A.W. and J.B. drafted portions of the manuscript and edited the paper. S.D. conceived of experiments, designed experiments, interpreted results and assumed primary responsibility for writing the manuscript.

involves nicking at the junction between the RSS and the coding sequence, followed by transesterification to produce a blunt, 5′-phosphorylated signal end and a coding end that terminates in a hairpin. Under physiologic conditions cleavage requires the pairing of a 12-RSS with a 23-RSS, so that recombination between like segments is suppressed (Schatz and Swanson, 2011).

V(D)J recombination acts in an ordered, locus-specific fashion during lymphoid development. In the B lineage, for example, the immunoglobulin heavy chain (IgH) locus is rearranged before the light chain loci and assembly of an Ig heavy chain gene proceeds by sequential D-to-J_H and V_H-to-DJ_H joining (Alt et al., 1984). Productive rearrangement suppresses further recombination at the IgH locus, thereby enforcing monoallelic expression of Ig heavy chain (Jung et al., 2006). The ability of gene segments to undergo V(D)J recombination is positively correlated with histone modifications characteristic of active chromatin, including hypermethylation of histone H3 at lysine 4 (Chakraborty et al., 2007; Goldmit et al., 2005; Liu et al., 2007; Matthews et al., 2007; Morshead et al., 2003; Subrahmanyam et al., 2012).

RAG-1 and RAG-2 are 1040 and 527 amino acid residues long, respectively. Although the canonical non-core region of RAG-2, comprising residues 387 through 527, is dispensable for DNA cleavage in vitro, removal of this region is associated with decreased recombination frequency (Steen et al., 1999) and increased aberrant recombination in vivo (Sekiguchi, 2001; Talukder et al., 2004). Interpretation of these effects is complicated by the presence of domains within the RAG-2 non-core region that support destruction at the G1-S transition (Jiang et al., 2005; Lee and Desiderio, 1999; Li et al., 1996; Zhang et al., 2011), nuclear import (Ross et al., 2003) and binding to H3K4me3 (Liu et al., 2007; Matthews et al., 2007; Ramon-Maiques et al., 2007). This last function is served by a plant homeodomain (PHD) finger spanning residues 415 through 487 (Callebaut and Mornon, 1998; Ramon-Maiques et al., 2007). Binding of H3K4me3 by the PHD finger promotes recombination in vivo (Liu et al., 2007; Matthews et al., 2007) and H3K4me3-bearing peptides stimulate DNA cleavage by RAG in vitro (Grundy et al., 2010; Shimazaki et al., 2009), suggesting that H3K4me3 is an allosteric activator of the V(D)J recombinase.

Paradoxically, removal of the RAG-2 non-core region impairs V(D)J recombination less severely than does selective mutation of the PHD finger (Cuomo and Oettinger, 1994; Sadofsky et al., 1994). Moreover, core RAG-2 supports D-to-J_H joining in vivo (Akamatsu et al., 2003; Kirch et al., 1998; Liang, 2002), while the full-length RAG-2(W453A) mutant, which is unable to bind H3K4me3, does so only weakly (Liu et al., 2007). These observations suggested the presence within RAG-2 of an autoinhibitory domain that is absent from the core fragment. We now uncover an autoregulatory region within RAG-2 that imposes allosteric control on V(D)J recombination. Disruption of autoinhibition mimics engagement of H3K4me3. Our observations support a model in which epigenetic control of RAG is enforced by an autoinhibitory domain whose action is relieved by active chromatin.

RESULTS

Identification of an autoinhibitory domain within the RAG-2 non-core region

We reasoned that an autoinhibitory domain would be identifiable by second site mutations that rescue the activity of RAG-2(W453A). We therefore scanned the entire canonical non-core region of RAG-2(W453A) with clustered alanine substitutions of 9 or 10 amino acid residues each. In a preliminary screen two contiguous secondary mutations, 388/396A_9 and 397/405A_9, rescued RAG-2(W435A) in an assay for V(D)J recombination (data not shown). We therefore constructed RAG-2 mutants bearing a clustered alanine substitution spanning residues 388 through 405 alone [RAG-2(388/405A_{18})] or in the presence of W453A [RAG-2(388/405A_{18}, W453A)] (Fig. S1A). The activity of RAG-2(W453A) in an assay for signal joining was impaired relative to wild-type, as reported (Liu et al., 2007). In contrast, the RAG-2(388/405A_{18}, W453A) double mutant exhibited no such reduction (Fig. 1A). Moreover, the RAG-2(388/405A_{18}) single mutant was significantly more active than wild-type (Fig. 1A). Differences in protein accumulation did not account for the effects of the 388/405A_{18} and W453A mutations (Fig. S1B). The gain of function associated with the 388/405A_{18} mutation was consistently observed in separate assays for signal joining (Fig. 1A, B and Fig. S1D, E), in an assay for coding joining (Fig. S1F) and in combination with a mutation (T490A) that uncouples RAG-2 accumulation from the cell cycle (Fig. S1G), suggesting that stimulation is independent of cell cycle-dependent control. The 388/405A_{18} mutation had no apparent effect on the precision of signal joining (Fig. S1H, I).

To define the amino-terminal boundary of the autoinhibitory domain we extended alanine scanning mutagenesis into the canonical core region of RAG-2 (Fig. S1A). RAG-2(370/387A_{18}) exhibited a gain-of-function phenotype similar to that of RAG-2(388/405A_{18}), while RAG-2(352/369A_{18}) was similar to wild-type and RAG-2(334/351A_{18}) did not support recombination (Fig. 1B). Mutations carboxy-terminal to residue 405 failed to confer a gain of function (Fig. 1B). The 370/387A_{18} mutation was not associated with increased accumulation of RAG-2 (Fig. S1C). These results are consistent with the presence of an autoinhibitory domain between amino acid residues 370 and 405 of RAG-2. The stimulatory effects of the 370/387A_{18} and 388/405A_{18} mutations were similar, and we performed subsequent assays with the latter.

Disruption of autoinhibition uncouples recombination of endogenous gene segments from H3K4me3 recognition

We employed a qualitative assay to determine whether disruption of the putative RAG-2 autoinhibitory domain could bypass the dependence of endogenous D-to-J_H joining on H3K4me3 recognition. To do so we expressed wild-type RAG-2, RAG-2(388/405A_{18}), RAG-2(W453A) or RAG-2(388/405A_{18}, W453A) in a RAG-2-deficient pro-B cell line using a retroviral vector that confers puromycin resistance. At 25 days of selection DSP2-to-J_H joining was assayed (Liu et al., 2007). Rearrangements were detected in cells transduced with core RAG-2, wild-type RAG-2 or RAG-2(388/405A_{18}) (Figure 1C, lanes 3–5). Rearrangements were profoundly reduced in cells transduced with RAG-2(W453A) (Figure 1C, lane 6). The debilitating effect of the W453A mutation was reversed, however, by mutation of residues 388–405 (Figure 1C, lane 7), consistent with the interpretation that

relief of autoinhibition bypasses the dependence of endogenous V(D)J recombination on recognition of H3K4me3 by RAG-2. Similar results were observed in two additional, independent transduction experiments (Fig. S1J, K).

Robust stimulation of RAG activity by exogenous H3K4me3 upon removal of endogenous H3K4me3

Although exogenous H3K4me3 has been shown to stimulate DNA cleavage by RAG, the responsiveness of standard RAG preparations has been inconsistent, suggesting variable contamination with endogenous H3K4me3. Indeed, standard amylose affinity preparations of MBP-tagged RAG fusion proteins (Fig. 1D, E) contained H3K4me3 (Fig. S2A, lanes 7 and 8). When we performed sonication before amylose affinity chromatography (Raval et al., 2008), contaminating H3K4me3 was removed (Fig. S2A, lanes 1 – 3). All RAG preparations employed hereafter were depleted of endogenous H3K4me3 in this way.

We assessed the effect of exogenous H3K4me3 on DNA cleavage by RAG in the absence of endogenous H3K4me3. Here we employed a version of RAG-1 lacking the amino-terminal non-core region but retaining the carboxy-terminal non-core region (cR1ct-MH, Fig. 1D) because RAG complexes containing cR1ct-MH are more robustly stimulated by H3K4me3 than complexes containing canonical core RAG-1 (Grundy et al., 2010), and because we obtained complexes containing cR1ct-MH in at least 20-fold greater yield than complexes containing full-length RAG-1. Full-length RAG-2 (fR2-MH, Fig. 1E) and cR1ct-MH fusion proteins were coexpressed and copurified (Fig. S2B) free of detectable endogenous H3K4me3 (Fig. S2A, lanes 4 – 6). This RAG complex was assayed for coupled cleavage of a radiolabeled 12-RSS substrate in the presence of unlabeled 23-RSS substrate and increasing amounts of a histone H3-derived peptide containing trimethylated lysine 4 (H3K4me3) or unmethylated lysine 4 (H3K4me0). Accumulation of nicked and hairpin products was stimulated in a dose-dependent fashion by H3K4me3, but not by H3K4me0 (Fig. 1F, G, upper panel). The yield of hairpin end-products showed about 4.5-fold maximal stimulation with half-maximal stimulation occurring at 0.6 – 1.25 μM H3K4me3. The yield of nicked intermediates was also stimulated by addition of H3K4me3 (Fig. 1G, lower panel); because these intermediates are obligatory, irreversible precursors of hairpins we deduce that H3K4me3 stimulates nicking. A reciprocal coupled cleavage assay using radiolabeled 23-RSS substrate and an unlabeled 12-RSS partner showed similar stimulation by H3K4me3 (Fig. S2C, D). Thus, soluble H3K4me3 robustly stimulates DNA cleavage by RAG that has been depleted of endogenous H3K4me3.

RAG-2(388/405A$_{18}$) exhibits increased basal activity but remains responsive to H3K4me3

The ability of the 388/405A$_{18}$ mutation to rescue activity of a PHD finger mutant was consistent with (1) disruption of an autoinhibitory domain whose action in the wild-type protein is relieved by H3K4me3 or (2) disruption of a separate mode of autoinhibition whose action is independent of H3K4me3 binding. To test these possibilities, we assayed wild-type RAG-2, RAG-2(W453A), RAG-2(388/405A$_{18}$) and RAG-2(388/405A$_{18}$, W453A) (Fig. 1E) for responsiveness to H3K4me3 in a coupled cleavage assay.

Equivalent amounts of active RAG tetramer, as determined by burst kinetic analysis (Fig. S3), were assayed for coupled cleavage of a radiolabeled 12-RSS in the presence of increasing concentrations of H3K4me0 or H3K4me3 (Fig. 2A). As expected, H3K4me3 stimulated hairpin formation by wild-type RAG: at 4 μM H3K4me3 the yield of hairpin product was more than 10 fold greater than in the absence of peptide (Fig. 2B, right panel). Stimulation was specific, as H3K4me0 had no effect (Fig. 2B, left panel). RAG-2(W453A) exhibited basal activity similar to that of wild-type (Fig. 2B, left panel), but was unresponsive to H3K4me3 (Fig. 2B, right panel), indicating that an intact PHD finger is required for stimulation. Consistent with its ability to rescue the recombination activity of RAG-2(W453A) in vivo, the 388/405A$_{18}$ mutation was associated with increased basal cleavage activity, either alone or in combination with W453A (Fig. 2B, left panel). Despite this increase in basal activity, RAG-2(388/405A$_{18}$) was stimulable by H3K4me3 (Fig. 2B); responsiveness required an intact PHD finger, as RAG-2(388/405A$_{18}$, W453A) was not stimulated (Fig. 2B, right panel). Consistent with these observations, RAG-2 fragments bearing the W453A and the 388/405A$_{18}$, W453A double mutation failed to bind H3K4me3, while a fragment bearing the 388/405A$_{18}$ mutation retained the ability to bind (Fig. S4A, B). Taken together, these observations indicate: (1) that the 388/405A$_{18}$ gain-of-function mutation confers increased basal cleavage activity in vitro but (2) that this mutation provides partial relief of autoinhibition, sparing one or more additional inhibitory functions that can be relieved by H3K4me3 binding.

Tetramers composed of full-length RAG-1 and full-length RAG-2 are largely insoluble. For this reason quantitative studies of RAG activity have generally employed the more soluble truncated forms of RAG-1, RAG-2 or both. Nonetheless, we were able to purify sufficient full-length protein to determine that full-length RAG-1 (flR1-MH; Fig. 1D), in complex with RAG-2(388/405A$_{18}$) or RAG-2(388/405A$_{18}$, W453A), exhibits increased basal nicking activity relative to a complex with RAG-2(W453A) (Fig. S4C). Moreover, full-length RAG-1, in complex with RAG-2(388/405A$_{18}$), is stimulable by H3K4me3 in a PHD-dependent manner (Fig. S4C). The elevated basal activity of the 388/405A$_{18}$ mutant and its responsiveness to H3K4me3 are consistent with the results of Fig. 2B.

Stimulatory effect of H3K4me3 on substrate binding

The stimulatory effect of the 388/405A$_{18}$ mutation could result from increased affinity for substrate, increased catalytic activity or both. To distinguish these possibilities we assessed substrate binding and catalysis. To measure affinity for DNA substrate, a 12-RSS fragment was incubated with increasing concentrations of wild-type RAG in the presence of 4 μM H3K4me0 or H3K4me3 peptide. Incubation was carried out in the presence of Ca^{++}, which supports the binding of RAG to substrate in the absence of DNA cleavage. The fraction of total substrate remaining in the unbound state was determined (Fig. 3A) and expressed as a function of active RAG concentration (Fig. 3C), as defined by burst kinetics under the assumption that the active unit is a heterotetramer of composition (RAG-1)$_2$(RAG-2)$_2$ (Yu and Lieber, 2000). Dissociation constants, K_D, were determined (see Experimental Procedures). The addition of H3K4me3 was accompanied by an increase in the affinity of wild-type RAG for substrate DNA, relative to control; in contrast, the affinity of RAG-2(388/405A$_{18}$) for a 12-RSS substrate was similar in the presence of H3K4me0 or

H3K4me3 (Fig. 3B, D). We also performed direct comparisons of substrate binding by each RAG species in the presence of H3K4me0 (Fig. 3E) or H3K4me3 (Fig. 3F). In the presence of control peptide the affinities (K_D) of RAG-2(388/405A$_{18}$) and wild-type RAG for substrate were estimated at 88 nM and 242 nM, respectively (Fig. 3G and Table S1). In the presence of H3K4me3, wild-type RAG and RAG-2(388/405A$_{18}$) bound substrate with an estimated K_D of 76 nM and 84 nM, respectively (Fig. 3H), similar to the affinity of RAG-2(388/405A$_{18}$) for substrate in the presence of H3K4me0. Thus the 388/405A$_{18}$ mutation confers a constitutive increase in substrate binding affinity by RAG independent of the presence of H3K4me3.

H3K4me3 and the RAG-2 388/405A$_{18}$ mutation stimulate catalysis of DNA cleavage

Because the 388/405A$_{18}$ mutation uncoupled the high affinity state from H3K4me3 binding, we were able to assess the effect of H3K4me3 on k_{cat} in the absence of its effect on K_D. We assayed nicking of a 12-RSS substrate at concentrations of 10 nM to 60 nM by RAG-2(388/405A$_{18}$) in complex with cR1ct-MH. Reactions were carried out at an active RAG tetramer concentration of 1.5 nM in the presence of 4 μM H3K4me0 or H3K4me3 peptide (Fig. 4A). Following determination of V_{max} (Fig. 4B and C), k_{cat} was estimated (Experimental Procedures). In the presence of H3K4me0, RAG-2(388/405A$_{18}$) supported nicking with an apparent k_{cat} of 4.95 min^{-1}, which increased to 7.06 min^{-1} in the presence of H3K4me3 (Fig 4C and Table S1). In comparison, we observed turnover rates of 0.83 min^{-1} and 3.76 min^{-1} for wild-type RAG-2 in the presence of H3K4me0 or H3K4me3, respectively (Fig. S4D, E and Table S1), consistent with previous estimates (Shimazaki et al., 2009). Thus the 388/405A$_{18}$ mutation is associated not only with increased affinity for substrate but also with a 6-fold increase in the basal k_{cat} for DNA nicking; the basal k_{cat} observed for RAG-2(388/405A$_{18}$) is similar to that observed for wild-type RAG-2 in the presence of H3K4me3. Nonetheless, RAG-2(388/405A$_{18}$) remains able to respond to H3K4me3 with an increase in catalytic rate. Taken together these results are consistent with a model in which the RAG-2 autoinhibitory domain suppresses substrate binding and catalysis through separable effects which are overcome by binding of H3K4me3.

DISCUSSION

The accessibility of antigen receptor loci to RAG is associated with epigenetic modifications characteristic of active chromatin, such as H3K4me3, whose recognition by RAG-2 promotes V(D)J recombination. The ability of H3K4me3 to stimulate cleavage of naked DNA by RAG has suggested that H3K4me3 relieves autoinhibition exerted by some feature of the RAG complex.

One hint as to the nature of this autoinhibitory function was provided by the ability of the RAG-2 core to support V(D)J recombination despite its inability to bind H3K4me3. We now reconcile these properties by showing that the basal activity of RAG is suppressed by an autoinhibitory domain that spans the boundary between the canonical core and non-core regions of RAG-2. Disruption of this autoinhibitory region uncouples V(D)J recombination from the requirement for H3K4me3 binding by RAG-2. Moreover, mutation of the autoinhibitory domain mimics the binding of H3K4me3 by increasing the affinity of RAG

for substrate and enhancing its catalytic rate. Our observations support a model in which the responsiveness of RAG to epigenetic stimulation is conferred by an autoinhibitory domain whose action is relieved upon binding of H3K4me3.

The ability of exogenous H3K4me3 to stimulate the coupled cleavage activity of wild-type RAG was dependent, as expected, on binding of H3K4me3 to the PHD finger of RAG-2. When autoinhibition was relieved by the 388/405A$_{18}$ mutation, basal cleavage activity in the absence of H3K4me3 was similar to that observed for wild-type RAG in the presence of saturating H3K4me3 peptide. H3K4me3 binding exerts at least two effects that contribute to enhanced RSS cleavage activity in vitro: increased affinity of RAG for substrate and faster catalysis. If the autoinhibitory domain confers allosteric activation by H3K4me3, then disruption of this domain would mimic the effects of H3K4me3 on substrate binding and catalysis. Indeed, the apparent K_D and k_{cat} for RAG-2(388/405A$_{18}$) in the absence of H3K4me3 were similar to those of wild-type RAG-2 in the presence of saturating H3K4me3. These observations indicate the presence of a functional element between residues 370 and 405 of RAG-2 that suppresses substrate binding and catalysis in the absence of H3K4me3. Our results are consistent with a model in which this autoinhibitory element maintains RAG in a state of low affinity for the RSSs until nearby transcriptional activation promotes allosteric activation through the deposition of H3K4me3.

The basal catalytic rate supported by RAG-2(388/405A$_{18}$) is similar to the maximally induced rate observed for wild-type RAG but is further increased in response to H3K4me3. While RAG-2(388/405A$_{18}$) supports a basal affinity for substrate that is also similar to the maximal induced affinity of wild-type RAG, H3K4me3 induces no further increase in affinity. Thus the effects of H3K4me3 on substrate affinity and catalysis are separable. We imagine several possible reasons that the 388/405A$_{18}$ mutant may remain responsive to H3K4me3 with respect to catalytic rate. First, because the boundaries of the autoinhibitory domain, as defined genetically, extend beyond the limits of the 388/405A$_{18}$ mutation, RAG-2(388/405A$_{18}$) may retain residual autoinhibitory activity. Second, there may exist additional suppressive elements within the RAG complex that dampen the catalytic rate for DNA cleavage in the absence of H3K4me3. Third, the 388/405A$_{18}$ mutation may exert a gain-of-function effect separate from or in addition to its ability to mimic H3K4me3 binding. In any event, the 388/405A$_{18}$ mutation permits RAG to bypass recognition of H3K4me3 in vivo and mimics the stimulatory effects of H3K4me3 on substrate binding and turnover rate in vitro.

Available data do not provide structural insight into autoinhibition or its relief by H3K4me3. One model would invoke direct competition between the inhibitory domain and H3K4me3 for binding to the PHD finger. This seems unlikely because the W453A mutation, which disrupts the H3K4me3 binding site, fails to relieve inhibition. Our results remain consistent with the possibility that the inhibitory domain exerts its suppressive effect through interactions with one or more regions of RAG distinct from the PHD finger. In this view, engagement of the PHD finger by H3K4me3 would relieve inhibition indirectly, perhaps through propagation of a conformational alteration within RAG.

The boundaries of the autoinhibitory domain lie within an acidic region of RAG-2, comprising residues 350 through 410. Neutralization of charge in this interval is associated with aberrant repair of RAG-mediated DNA breaks, decreased stability of RAG-signal end complexes (SECs) and genomic instability (Coussens et al., 2013). While these effects appear to reflect events occurring after RSS recognition and DNA cleavage, they may be explained in part by our results. An increase in genomic instability, for example, would be consistent with the uncoupling of substrate recognition and cleavage from H3K4me3 binding that we observe upon mutation of this region. A unifying hypothesis would suggest that the destabilization of SECs, and relaxation of repair pathway choice, are consequences of the structural alterations that uncouple RAG activity from H3K4me3 binding upon mutation of the autoinhibitory domain. For example, if formation of a stable SEC were to require disengagement of RAG from H3K4me3, then mutations that mimic the effect of H3K4me3 engagement, such as RAG-2 $388/405A_{18}$, could compromise SEC stability and appropriate repair of DNA ends.

EXPERIMENTAL PROCEDURES

Cell culture

NIH3T3 and HEK 293T cells were propagated in Dulbecco's modified Eagle's medium (DMEM) supplemented with 10% fetal bovine serum (FBS). Cells were maintained at 37°C in 5% CO_2.

Antibodies

Antibodies against the following proteins were used in this study: histone H3K4me3 (Millipore CMA-304); MBP (Santa Cruz sc-808); actin (Santa Cruz, sc-8432); and c-myc (Millipore CBL-430).

Oligonucleotide substrates

Two pairs of duplex oligonucleotides were used in RSS cleavage and binding assays: DAR39/40 (12-RSS) and DAR61/62 (23-RSS) (McBlane et al., 1995) or HL44/45 (12-RSS) and HL46/47 (23-RSS) (Shimazaki et al., 2012). Oligonucleotides were purified by gel electrophoresis and 5′ end-labeled where indicated with ^{32}P by T4 DNA polynucleotide kinase (New England Biolabs). Complementary oligonucleotides were annealed as described (Lu et al., 2008).

DNA binding assays

Varying amounts of RAG tetramer up to 0.3 μM were combined with 1 nM radiolabeled HL44/45 in binding buffer [25mM 3-(4-Morpholino)propane sulfonic acid-KOH pH7.0, 30 mM KCl, 30mM potassium glutamate, 6% glycerol, 0.1 mg/mL BSA, 4 mM $CaCl_2$, 1 mM DTT] at a reaction volume of 10 μl. After 20 min at 37°C, 4 μl of 50% glycerol were added and reactions were resolved on a composite 4%/8% non-denaturing gel as described (Zhao et al., 2009). Radiolabeled species were detected on a phosphorimager and the percent of total radioactivity present as free substrate at each RAG concentration was determined using ImageQuantNL (GE Healthcare). To determine the dissociation constant K_D, data were fitted by nonlinear regression to the equation

$$F=\frac{K_D^n}{K_D^n+[RAG]^n}$$

where F is the fraction of substrate that is unbound, K_D is the dissociation constant and n is the Hill coefficient. Nonlinear regression analysis was performed using GraphPad Prism v. 5.0 (GraphPad Software).

Determination of catalytic rate constants

Wild-type or mutant RAG complexes (1.5 nM active tetramer, as determined by burst kinetic analysis) was combined with HL44/45 at concentrations varying from 10 nM to 60 nM) in a buffer containing 25 mM 3-(4-Morpholino)propane sulfonic acid-KOH pH 7.0, 30 mM KCl, 30 mM potassium glutamate, 5 mM $MgCl_2$, 1 mM DTT, 1% glycerol and 0.1 mg/ml BSA in reaction volumes of 20 μl at 37°C. Aliquots (2 μl) were withdrawn at varying times up to 3 min and reactions were stopped by addition of 1 volume 90% formamide-TBE. Products were quantified as above. V_{max} was estimated by curve fitting to a Michaelis-Menton model (GraphPad Prism v. 5.0, GraphPad Software) and k_{cat} was determined from the relationship:

$$k_{cat}=\frac{V_{max}}{[RAG]_T}.$$

Expression constructs, Protein purification, Recombination assays, Burst kinetic analysis, Assays for coupled cleavage and Surface plasmon resonance are described under Supplemental experimental procedures.

Supplementary Material

Refer to Web version on PubMed Central for supplementary material.

Acknowledgments

We are grateful to Ranjan Sen (NIA-NIH) for stimulating discussions and Scheherezade Saddegh-Nasseri (Johns Hopkins University) for assistance with surface plasmon resonance measurements. This work was supported by grant R01 CA160256 from the National Cancer Institute and by a gift to the Institute for Cell Engineering at the Johns Hopkins University School of Medicine. C.L. was a Visiting Scientist of the Johns Hopkins-Fudan Visiting Scholar Program.

References

Akamatsu Y, Monroe R, Dudley DD, Elkin SK, Gartner F, Talukder SR, Takahama Y, Alt FW, Bassing CH, Oettinger MA. Deletion of the RAG2 C terminus leads to impaired lymphoid development in mice. Proc Natl Acad Sci U S A. 2003; 100:1209–1214. [PubMed: 12531919]

Alt FW, Yancopoulos GD, Blackwell TK, Wood C, Thomas E, Boss M, Coffman R, Rosenberg N, Tonegawa S, Baltimore D. Ordered rearrangement of immunoglobulin heavy chain variable region segments. The EMBO journal. 1984; 3:1209–1219. [PubMed: 6086308]

Callebaut I, Mornon JP. The V(D)J recombination activating protein RAG2 consists of a six-bladed propeller and a PHD fingerlike domain, as revealed by sequence analysis. Cell Mol Life Sci. 1998; 54:880–891. [PubMed: 9760994]

Chakraborty T, Chowdhury D, Keyes A, Jani A, Subrahmanyam R, Ivanova I, Sen R. Repeat organization and epigenetic regulation of the DH-Cmu domain of the immunoglobulin heavy-chain gene locus. Mol Cell. 2007; 27:842–850. [PubMed: 17803947]

Coussens MA, Wendland RL, Deriano L, Lindsay CR, Arnal SM, Roth DB. RAG2's Acidic Hinge Restricts Repair-Pathway Choice and Promotes Genomic Stability. Cell reports. 2013; 4:870–878. [PubMed: 23994475]

Cuomo CA, Oettinger MA. Analysis of regions of RAG-2 important for V(D)J recombination. Nucleic Acids Res. 1994; 22:1810–1814. [PubMed: 8208604]

Gellert M. V(D)J recombination: RAG proteins, repair factors, and regulation. Annu Rev Biochem. 2002; 71:101–132. [PubMed: 12045092]

Goldmit M, Ji Y, Skok J, Roldan E, Jung S, Cedar H, Bergman Y. Epigenetic ontogeny of the Igk locus during B cell development. Nat Immunol. 2005; 6:198–203. [PubMed: 15619624]

Grundy GJ, Yang W, Gellert M. Autoinhibition of DNA cleavage mediated by RAG1 and RAG2 is overcome by an epigenetic signal in V(D)J recombination. Proc Natl Acad Sci U S A. 2010; 107:22487–22492. [PubMed: 21149691]

Hesse JE, Lieber MR, Gellert M, Mizuuchi K. Extrachromosomal DNA substrates in pre-B cells undergo inversion or deletion at immunoglobulin V-(D)-J joining signals. Cell. 1987; 49:775–783. [PubMed: 3495343]

Jiang H, Chang FC, Ross AE, Lee J, Nakayama K, Nakayama K, Desiderio S. Ubiquitylation of RAG-2 by Skp2-SCF links destruction of the V(D)J recombinase to the cell cycle. Mol Cell. 2005; 18:699–709. [PubMed: 15949444]

Jung D, Giallourakis C, Mostoslavsky R, Alt FW. Mechanism and control of V(D)J recombination at the immunoglobulin heavy chain locus. Annu Rev Immunol. 2006; 24:541–570. [PubMed: 16551259]

Kirch SA, Rathbun GA, Oettinger MA. Dual role of RAG2 in V(D)J recombination: catalysis and regulation of ordered Ig gene assembly. The EMBO journal. 1998; 17:4881–4886. [PubMed: 9707447]

Lee J, Desiderio S. Cyclin A/CDK2 regulates V(D)J recombination by coordinating RAG-2 accumulation and DNA repair. Immunity. 1999; 11:771–781. [PubMed: 10626899]

Li Z, Dordai DI, Lee J, Desiderio S. A conserved degradation signal regulates RAG-2 accumulation during cell division and links V(D)J recombination to the cell cycle. Immunity. 1996; 5:575–589. [PubMed: 8986717]

Liang H, Hsu LY, Cado D, Cowell LG, Kelsoe G, Schlissel MS. The "dispensible" portion of RAG2 is necessary for efficient V-to-DJ rearrangement during B ad T cell development. Immunity. 2002; 17:639–651. [PubMed: 12433370]

Liu Y, Subrahmanyam R, Chakraborty T, Sen R, Desiderio S. A plant homeodomain in RAG-2 that binds Hypermethylated lysine 4 of histone H3 is necessary for efficient antigen-receptor-gene rearrangement. Immunity. 2007; 27:561–571. [PubMed: 17936034]

Lu H, Shimazaki N, Raval P, Gu J, Watanabe G, Schwarz K, Swanson PC, Lieber MR. A biochemically defined system for coding joint formation in V(D)J recombination. Mol Cell. 2008; 31:485–497. [PubMed: 18722175]

Matthews AG, Kuo AJ, Ramon-Maiques S, Han S, Champagne KS, Ivanov D, Gallardo M, Carney D, Cheung P, Ciccone DN, et al. RAG2 PHD finger couples histone H3 lysine 4 trimethylation with V(D)J recombination. Nature. 2007; 450:1106–1110. [PubMed: 18033247]

McBlane JF, van Gent DC, Ramsden DA, Romeo C, Cuomo CA, Gellert M, Oettinger MA. Cleavage at a V(D)J recombination signal requires only RAG1 and RAG2 proteins and occurs in two steps. Cell. 1995; 83:387–395. [PubMed: 8521468]

Morshead KB, Ciccone DN, Taverna SD, Allis CD, Oettinger MA. Antigen receptor loci poised for V(D)J rearrangement are broadly associated with BRG1 and flanked by peaks of histone H3 dimethylated at lysine 4. Proc Natl Acad Sci U S A. 2003; 100:11577–11582. [PubMed: 14500909]

Ramon-Maiques S, Kuo AJ, Carney D, Matthews AG, Oettinger MA, Gozani O, Yang W. The plant homeodomain finger of RAG2 recognizes histone H3 methylated at both lysine-4 and arginine-2. Proc Natl Acad Sci U S A. 2007; 104:18993–18998. [PubMed: 18025461]

Raval P, Kriatchko AN, Kumar S, Swanson PC. Evidence for Ku70/Ku80 association with full-length RAG1. Nucleic Acids Res. 2008; 36:2060–2072. [PubMed: 18281312]

Ross AE, Vuica M, Desiderio S. Overlapping signals for protein degradation and nuclear localization define a role for intrinsic RAG-2 nuclear uptake in dividing cells. Mol Cell Biol. 2003; 23:5308–5319. [PubMed: 12861017]

Sadofsky MJ, Hesse JE, Gellert M. Definition of a core region of RAG-2 that is functional in V(D)J recombination. Nucleic Acids Res. 1994; 22:1805–1809. [PubMed: 8208603]

Schatz DG, Swanson PC. V(D)J recombination: mechanisms of initiation. Annual review of genetics. 2011; 45:167–202.

Sekiguchi J, Whitlow S, Alt FW. Increased accumulation of hybrid V(D)J joins in cells expressing truncated versus full-length RAGs. Mol Cell. 2001; 8:1383–1390. [PubMed: 11779512]

Shimazaki N, Askary A, Swanson PC, Lieber MR. Mechanistic basis for RAG discrimination between recombination sites and the off-target sites of human lymphomas. Mol Cell Biol. 2012; 32:365–375. [PubMed: 22064481]

Shimazaki N, Tsai AG, Lieber MR. H3K4me3 stimulates the V(D)J RAG complex for both nicking and hairpinning in trans in addition to tethering in cis: implications for translocations. Mol Cell. 2009; 34:535–544. [PubMed: 19524534]

Steen SB, Han JO, Mundy C, Oettinger MA, Roth DB. Roles of the “dispensable” portions of RAG-1 and RAG-2 in V(D)J recombination. Mol Cell Biol. 1999; 19:3010–3017. [PubMed: 10082568]

Subrahmanyam R, Du H, Ivanova I, Chakraborty T, Ji Y, Zhang Y, Alt FW, Schatz DG, Sen R. Localized epigenetic changes induced by DH recombination restricts recombinase to DJH junctions. Nat Immunol. 2012; 13:1205–1212. [PubMed: 23104096]

Talukder SR, Dudley DD, Alt FW, Takahama Y, Akamatsu Y. Increased frequency of aberrant V(D)J recombination products in core RAG-expressing mice. Nucleic Acids Res. 2004; 32:4539–4549. [PubMed: 15328366]

Yu K, Lieber MR. The nicking step in V(D)J recombination is independent of synapsis: implications for the immune repertoire. Mol Cell Biol. 2000; 20:7914–7921. [PubMed: 11027262]

Zhang L, Reynolds TL, Shan X, Desiderio S. Coupling of V(D)J recombination to the cell cycle suppresses genomic instability and lymphoid tumorigenesis. Immunity. 2011; 34:163–174. [PubMed: 21349429]

Zhao S, Gwyn LM, De P, Rodgers KK. A non-sequence-specific DNA binding mode of RAG1 is inhibited by RAG2. J Mol Biol. 2009; 387:744–758. [PubMed: 19232525]

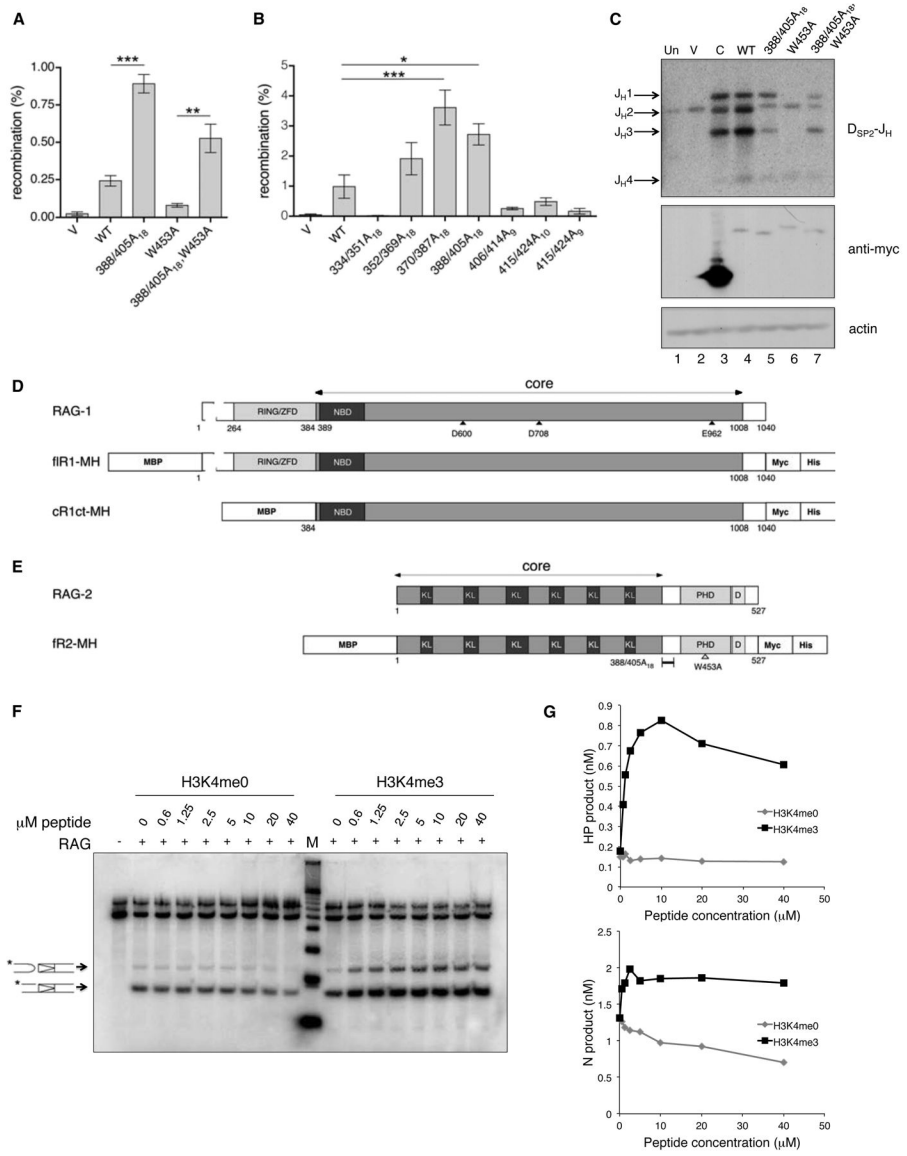

Figure 1.

Autoinhibition of RAG in vivo and stimulation of chromatin-depleted RAG by H3K4me3 in vitro. (A) Rescue of an inactivating PHD finger mutation. Recombination (%), frequency of signal joining in cells transfected with pJH200 (Hesse et al., 1987), full-length RAG-1 and vector (V), full-length wild-type RAG-2 (wt) or full-length RAG-2 mutants as indicated (mean ± S.E.M., n = 3 independent biological replicates, representing ≥ 500 ampicillin (amp)-resistant colonies per RAG-2 variant and ≥ 200 amp-resistant colonies for vector alone) Significant differences were determined by ANOVA: ***, $P < 0.001$; **, $P < 0.01$. (B) Mapping of the autoinhibitory domain. Signal joining (mean ± S.E.M., n = 3 independent biological replicates, representing ≥ 100 amp-resistant colonies per RAG-2 variant) was assayed using full-length RAG constructs and analyzed as in (A); ***, $P < 0.001$; *, $P < 0.05$. (C) Rescue of W453A by $388/405A_{18}$ in an assay for endogenous recombination. Top panel, assay for D_{SP2}-to-J_H joints in genomic DNA from uninfected

cells (Un) or cells transduced with the following: vector alone (V), core RAG-2 (C), full-length wild-type RAG-2 (wt) or full-length RAG-2 mutants. Positions of D_{SP2}-to-J_H recombinants are indicated at left. Middle and bottom panels, detection of myc-tagged RAG-2 species and actin, respectively, by immunoblotting. (D) Diagrams of wild-type RAG-1 (top), full-length RAG-1-MH (flR1-MH, middle) and core RAG-1ct-MH (cR1ct-MH, bottom). Amino acid residues at domain boundaries are numbered. The core is designated in dark gray. The RING-type zinc-finger domain (RING/ZFD) and the nonamer-binding domain (NBD) are indicated. Arrowheads, catalytic residues. MBP, Myc and His denote the maltose-binding protein, c-myc epitope and polyhistidine tags, respectively. (E) RAG-2 constructs for in vitro assays. Above, wild-type RAG-2. Below, full-length RAG-2 fusion protein. Amino acid residues at domain boundaries are numbered. The core is shown in dark gray. Kelch-like domains (KL), the PHD finger (PHD) and the degradation signal (D) are indicated. MBP, Myc and His are as defined in (D). Positions of mutations are marked below. (F) Stimulation of H3K4me3-depleted RAG by exogenous H3K4me3. Coupled cleavage reactions contained radiolabeled 12-RSS and unlabeled 23-RSS. Additions of RAG and H3K4me0 or H3K4me3 are indicated above. Positions of hairpin (HP) and nicked (N) products are indicated by arrows. M, 10 bp marker ladder. Uncleaved substrate migrates as a doublet, likely as a result of incompletely melted secondary structure. (G) Accumulation of hairpin product (upper panel) or nicked intermediates (lower panel) at 1 hr is plotted in nM as a function of H3K4me0 (gray diamonds) or H3K4me3 (black squares) concentration. Data in (F) and (G) are representative of more than three experiments.

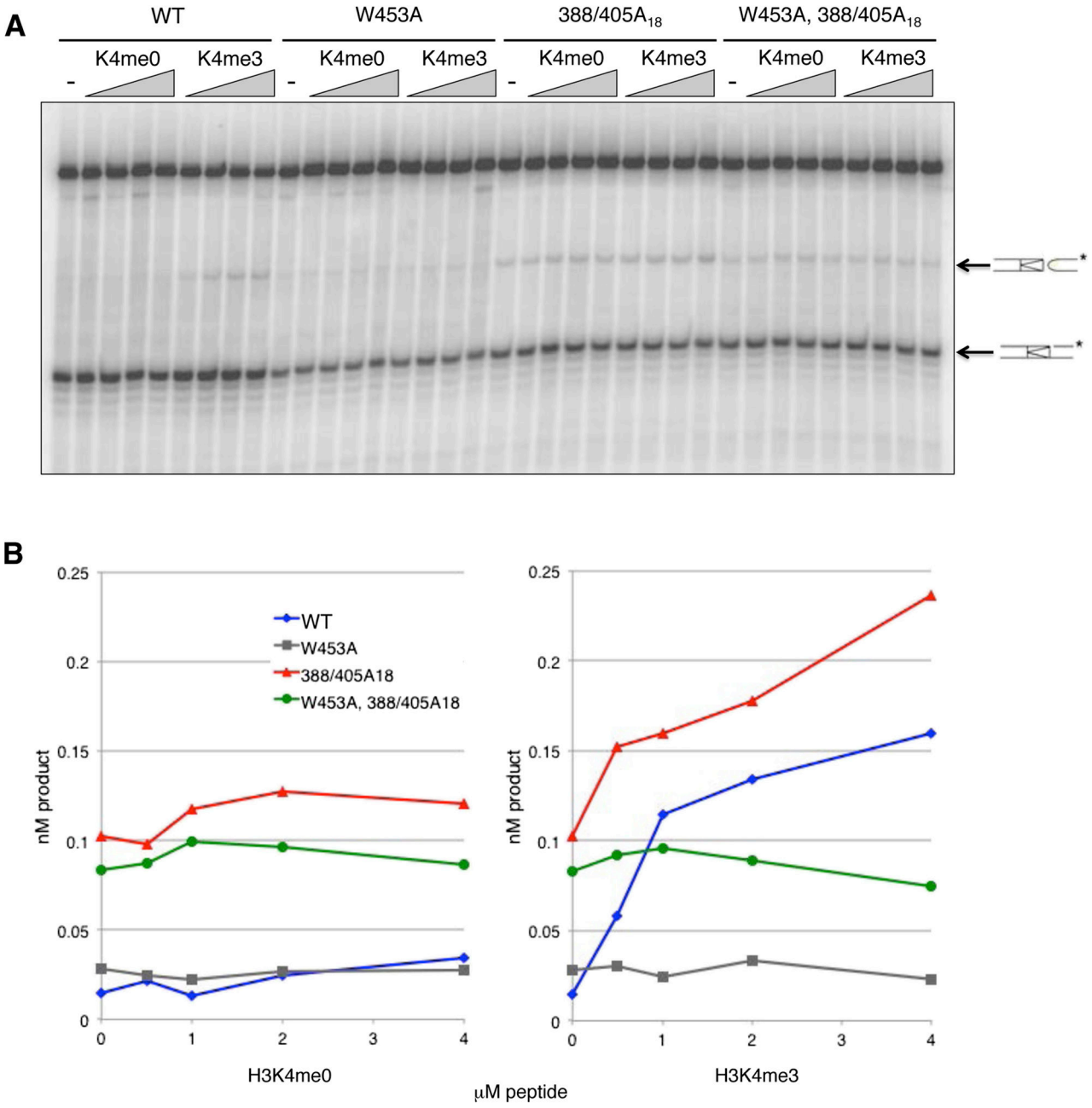

Figure 2.

Mutation of the RAG-2 autoinhibitory domain increases coupled cleavage activity. (A) Coupled cleavage reactions contained radiolabeled 12-RSS, unlabeled 23-RSS and wild-type (wt) RAG-2 or RAG-2 mutants as defined at top. K4me0 and K4me3, reactions supplemented with 0.5, 1, 2 or 4 μM H3K4me0 or H3K4me3 peptide; -, reactions lacking peptide. Positions of hairpin (HP) and nicked (N) products are indicated by arrows. (B) Accumulation of hairpin product at 1 hr (nM product) is plotted as a function of the concentration of H3K4me0 (left) or H3K4me3 (right). Blue diamonds, wild-type RAG-2; gray squares, RAG-2(W453A); red triangles, RAG-2(388/405A$_{18}$); green circles,

RAG-2(W453A, 388/405A_{18}). Data in (A) and (B) are representative of more than three experiments.

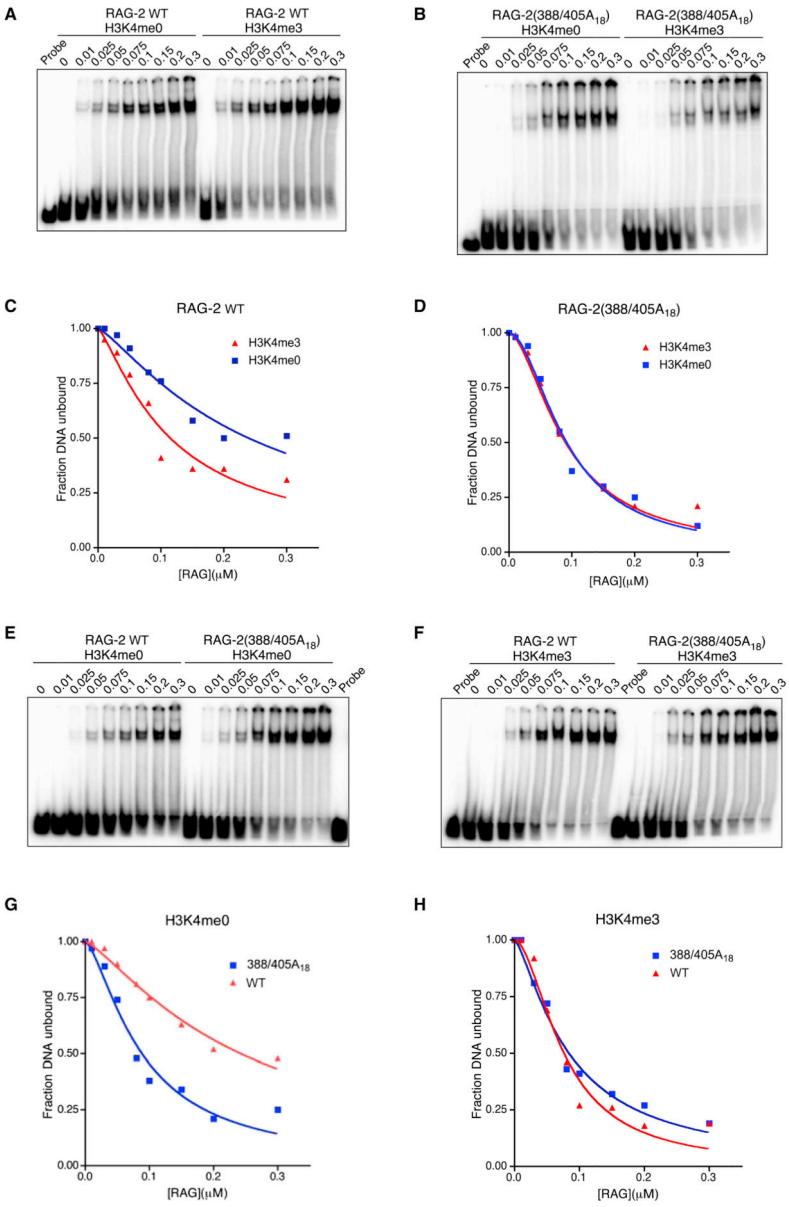

Figure 3.

The RAG-2 388/405A_{18} mutation mimics the stimulatory effect of H3K4me3 on RAG-RSS binding. (A) Electrophoretic mobility shift assay (EMSA) for binding of wild-type RAG to a consensus 12-RSS in the presence of H3K4me0 or H3K4me3 peptide as indicated at top. Probe, 12 RSS incubated in the absence of RAG. The concentration, in μM, of active RAG in each binding reaction is indicated above the lane. (B) EMSA as in (A) except that RAG-2(388/405A_{18}) was substituted for wild-type RAG-2. (C) H3K4me3 reduces the K_D of RAG-RSS binding. The fraction of free probe (fraction DNA unbound) in each binding reaction of panel (A) was plotted as a function of active RAG concentration. Data from reactions containing H3K4me0 and H3K4me3 are indicated by blue squares and red triangles, respectively. (D) The RAG-2 388/405A_{18} mutation relieves responsiveness of RAG-RSS binding to H3K4me3. The fraction of free probe (fraction DNA unbound) in each

binding reaction of panel (B) is plotted as in (C). (E) EMSA for binding of wild-type RAG (left) or RAG-2(388/405A_{18}) (right) to a consensus 12-RSS in the presence of H3K4me0. Probe, 12 RSS incubated in the absence of RAG. The concentration of active RAG in each reaction is indicated above the lane. (F) EMSA as in (E) except that H3K4me3 was substituted for H3K4me0. (G) The RAG-2 388/405A_{18} mutation increases basal affinity of RAG for RSS in the absence of H3K4me3. The fraction of free probe (fraction DNA unbound) in each binding reaction of panel (E) was plotted as a function of active RAG concentration. Data from reactions containing RAG-2(388/405A_{18}) and wild-type RAG-2 are indicated by blue squares and red triangles, respectively. K_D estimates for wild-type (wt) and mutant (mut) proteins are indicated. (H) The fraction of free probe (fraction DNA unbound) in each binding reaction of panel (F) is plotted as in (G). Data in (A), (B), (E) and (F) are representative of three experiments.

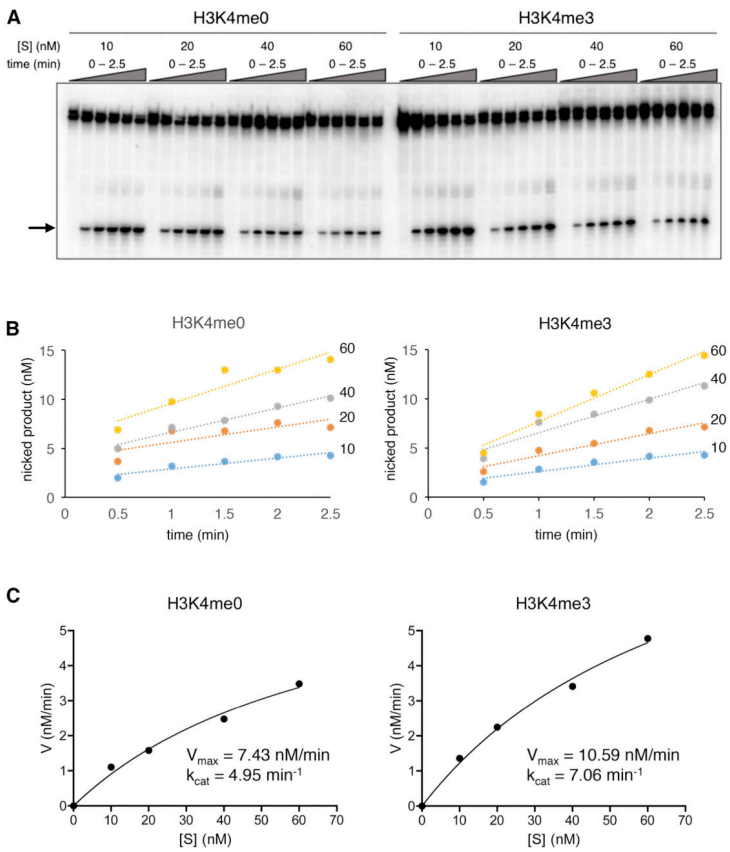

Figure 4.

Disruption of the RAG-2 autoinhibitory domain mimics the stimulatory effect of H3K4me3 on catalytic rate. (A) Assay for RSS nicking. Reactions contained 1.5 nM RAG-2(388/405A$_{18}$) and 12-RSS substrate HL44/45 at 10, 20, 40 or 60 nM. Reactions were supplemented with 4 μM H3K4me0 or H3K4me3 peptide as indicated at top. Accumulation of nicked product (arrow) was assayed at times ranging from 0 to 2.5 min. (B) Concentration of nicked product as determined in (A) is plotted against time for each substrate concentration. Blue, 10 nM; orange, 20 nM; gray, 40 nM; and yellow, 60 nM. Left, reactions containing H3K4me0; right, reactions containing H3K4me3. (C) Reaction velocity (V) is plotted in nM/min as a function of substrate concentration ([S]). V_{max} was determined by non-linear regression analysis (Experimental Procedures); $k_{cat} = V_{max}/[RAG]_T$, where $[RAG]_T$ is the total concentration of active RAG tetramer. Data are representative of two experiments.